J Porous Mater (2008) 15:21–27
DOI 10.1007/s10934-006-9047-5

Synthesis and characterization of porous TiO_2 with wormhole-like framework structure

Arun Narayanaswamy · James McBride · Laura A. Swafford · Sarit Dhar · John D. Budai · Leonard C. Feldman · Sandra J. Rosenthal

Received: 4 May 2006 / Revised: 4 May 2006 / Published online: 26 January 2007

Abstract A fast and reliable synthetic route for preparing contaminant-free porous TiO_2 with a wormhole-like framework and close packed macropores is demonstrated based on a sol-gel process involving acid hydrolysis of an alkoxide in the presence of a cationic surfactant. Powder X-ray diffraction (XRD) and transmission electron microscopy (TEM) measurements have been used to characterize the porous structure and the crystallinity. The XRD patterns, TEM and scanning electron microscopy (SEM) images confirm that these materials have disordered wormhole-like topology with close-packed nearly hexagonal macropores. The mesopore diameters and surface area of titanium dioxide, evaluated from the N_2-sorption isotherms, indicate average pore diameters of about 7 and 6 nm and surface areas of about 100 and 335 m^2/g, for as-prepared and calcined samples at 400°C.

Keywords Mesoporous · Titanium dioxide · Acid hydrolysis · XRD · TEM · Macropores

A. Narayanaswamy · J. McBride · L. A. Swafford · S. J. Rosenthal (✉)
Department of Chemistry, Vanderbilt University, Nashville, TN, USA
e-mail: sandra.j.rosenthal@vanderbilt.edu

S. Dhar · L. C. Feldman
Department of Physics and Astronomy, Vanderbilt University, Nashville, TN 37235, USA

J. D. Budai
Oak Ridge National Laboratory , Oak Ridge, TN 37831-6030, USA

1 Introduction

Since the discovery of surfactant-organized silicas and silicates in the early 1990s [1–3], there has been extensive research in the field of mesoporous solids, motivated by the promise of these materials as catalyst supports, optical materials, sensors, low *k*-dielectrics, membranes and selective adsorbents [3–5]. Most studies on the preparation of mesoporous materials are focussed on silica, most likely because it is easier to synthesize than mesoporous transition metal oxides, whose pore walls tend to collapse during calcinations [6]. In fact, mesoporous transition metal oxides are of particular interest in the materials research because of their variable oxidation states (a property not possessed by silicates), a capacity which often leads to unusual magnetic, electronic and catalytic properties [7,8]. Nonetheless, a few research efforts have suggested that it is possible to synthesize mesoporous materials based on transition metal oxides [9–11].

Semiconducting transition metal oxides participate in a variety of photocatalytic reactions. Titanium dioxide (TiO_2) is the one of the most studied semiconductors because of its numerous applications in the chemical [12], medical [13], biological [14], environmental [12, 15] and solar energy fields [16]. High surface area mesostructured TiO_2 is well known for its high catalytic activity, especially for photocatalytic properties, which have been investigated for many years and widely used in the photocatalytic oxidation of toluene, 1-butene etc. [17–18]. The use of titanium dioxide in photocatalysis processes is dependent on the absorption characteristics, which allow it to absorb photons of UV light, producing reactive electron-hole pairs that can react with surrounding materials [12, 15, 19].

The durability and stability of TiO_2 during such reactions make it an ideal material for any application where the material is to be used continuously without frequent replacement. In a majority of these applications accessibility to a crystalline surface is of prime importance [20]. Therefore the production of an open, highly porous titanium dioxide network in either the anatase, rutile or brookite crystalline phases is desirable because (1) the high surface area allows maximum contact between the TiO_2 network and the reaction medium and (2) the continuity of the network prevents traps from depleting its efficiency.

The success in obtaining a specific mesoporous metal oxide depends on two factors: (1) the occurrence of a three-dimensional mesophase and (2) the stability of the metal oxide framework upon the removal of the surfactant species. The stability of a mesostructure depends on the extent of the condensation and crystallinity of the inorganic walls. A higher degree of polymerization tends to impart improved thermal stability. The polymerization of the inorganic species is normally achieved by adjusting the pH and the reaction temperature. Further, the interaction between the surfactant and the inorganic wall should not be too strong, so that the mesostructure assembly can take place and the surfactant can be removed easily without damage to the integrity of the channel walls. For this purpose, hydrogen bonding, and/or weak coordination bonds are more preferred than electrostatic interactions and covalent bonding.

To date, several preparative approaches employing a supramolecular templating mechanism have been reported for the preparation of mesoporous titanium dioxide [11, 21–28]. In general ionic surfactants, nonionic surfactants and block copolymers have been exploited as templates to direct the formation of mesoporous titania materials based on electrostatic and hydrogen bonding interactions [21, 22]. The preparation of pure mesoporous titania was first reported by Antonelli's group in 1995 [11]. It was obtained by a modified sol-gel process, using alkylphosphate surfactant as the template. The disadvantage in this method was that phosphorous from the template was bound so strongly to the molecular sieve that it could not be removed completely by either calcination or solvent extraction and the mesostructure of the sieve underwent partial collapse. This limited its possible use as a catalyst or catalyst support; for example, one of the reasons for the relative low photocatalytic activity of these materials is attributed to the poisoning of the catalytic surface sites by the residual phosphorous [22, 23]. In an attempt to solve the problem of activity-destroying phosphorous, Antonelli et al. [26] reported the preparation of mesoporous TiO_2 using dodecyl amine as the directing agent. While this solved the problem of residual phosphorous, the porous structure remained unstable after calcination. Sanchez et al have reported the synthesis of mesoporous TiO_2 with hexagonal, cubic and wormlike structures using CTAB as the surfactant [29–32]. There are numerous reports by Vansant et al. on the synthesis of mesoporous titania using amines as surfactants [33–36].

In this manuscript, we describe a fast and reliable method for the synthesis of hybrid titania-based materials with a worm-like framework and high surface area in an easy and reproducible manner. This material is interesting because of its large and accessible pore surface owing to the presence of close-packed nearly hexagonal macropores. The hybrid materials are ''titaniatropic''(i.e., hybrid liquid–crystalline phases; cf. ref. 37), flexible mesostructures that are only partially condensed. These mesostructured phases are composed of preformed titania nano building blocks (NBB) and thermal treatment of these precursors leads to high surface-area phosphate-free TiO_2. The as-prepared and calcined samples were characterized by wide angle and low angle X-ray diffraction (XRD), transmission electron microscopy (TEM), Rutherford backscattering spectroscopy and N_2 adsorption–desorption experiments.

2 Experimental

2.1 Chemicals

The surfactant used in this study was cetyl-trimethylammonium bromide, $[C_{16}H_{33}N^{+}(CH_3)_3]Br^{-}$ (CTAB), the titanium source was tetraethylorthotitanate (TEOT), the source of acid was hydrochloric acid and the co-solvent was methanol, all of which were of analytical grade and purchased from Aldrich Chemical Co. All chemicals were used as received.

2.2 Synthesis

Aqueous micellar precursor solutions containing 5–12 wt% CTAB were heated gently (30–40°C) to dissolve the surfactant. In a typical synthesis 1.7 g of CTAB was dissolved in 25 ml of deionised water. The inorganic titanium precursor was prepared by dissolving 5.8 g of TEOT in 3.2 g of aqueous HCl (37 wt%) and 9 g of methanol (CH_3OH). The solution was heated at 50°C for 3 h, to obtain a clear solution. Appropriate amounts of the surfactant and titanate precursor solutions ($[H_2O]/[Ti] = 75$) were combined

at room temperature and samples stirred for 3 h to allow equilibration. The resulting sol solution was gelled in an open petri dish at 40°C in air for 4 days during which the titanium precursor hydrolyzes and polymerizes into a titanium oxide network. Alternatively the sol solution can be used to prepare thin films by spin coating. The surfactant species was then removed by calcination in the following manner. Calcination was done with a slow heating rate of 1°/min. The samples were first heated under flowing N_2 from room temperature to 400°C over 8 h and subsequently held for 6 h. The gas was then changed to O_2 for 6 h at 400°C, followed by cooling over 4 h to room temperature under flowing O_2.

2.3 Characterization

Wide-angle XRD measurements were obtained on a Scintag PADX diffractometer using Cu Kα radiation. Low angle XRD measurements were obtained using a Rigaku rotating anode Cu Kα X-ray source, a vertically focussing LiF monochromator, and a Huber four-circle diffractometer. Mesoporous TiO_2 samples approximately 1 micron thick were deposited on Si(001) substrates in order to minimize background scattering, and the samples were then mounted with the surface normal parallel to the φ axis of the diffractometer. A high-resolution Ge(111) analyzer crystal was placed after the sample and θ–2θ scans were used to search for long-range mesoscopic order.

TEM and high resolution transmission electron miscroscopy (HR-TEM) studies were carried out on a Phillips CM 20 electron microscope operating at 200 keV. The samples for TEM were prepared by dispersing mesoporous TiO_2 powder in isopropanol; the dispersion was then dropped onto ultra-thin, carbon-coated copper grids.

Scanning electron microscopy (SEM) studies were carried out on a Hitachi S-4200 electron microscope operating at 30 keV. Samples for SEM were prepared by sprinkling powdered samples onto a double-sided carbon tape stuck to an aluminum stub. Nitrogen adsorption and desorption isotherms were measured at 77 K using a Quantachrome Nova 1,000 system after the samples were vacuum dried at 150°C overnight.

Rutherford backscattering spectroscopy (RBS) analysis was performed using a 1.8 MeV van de Graaf generator. Samples for RBS were prepared by dispersing the powders in acetone and dropping them onto a 1 cm^2 graphite or Si(001) substrates and wicking off any excess solution. Spectra were generated using He^+ as the ion source.

3 Results and discussion

Figure 1 displays the wide-angle and low-angle XRD patterns of mesoporous titania. The wide-angle XRD pattern is characteristic of the body-centred tetragonal anatase phase (JCPDS no. 21-1272) of TiO_2 and the intensity ratios show that the crystallites are randomly oriented. The broad diffraction peaks arise from the nano-scale size of the crystals comprising the sample. The crystallite size as calculated from the Scherrer equation for the 101 reflection, is about 5nm. In the measurement range 0.5–8°, as shown in Fig. 1b, no low-angle peaks are observed, suggesting that the materials have a disordered mesostructure without long-range order in the mesopore arrangement. Similar XRD patterns have been observed by other groups [27, 38].

The TEM image of a calcined sample, as shown in Fig. 2a, demonstrates the disordered worm-like pore structure of the TiO_2. In this system, the pores (light areas) are formed by the agglomeration of TiO_2 nanocrystals. The accessible pores are connected randomly and there is an absence of discernible long-range order in the pore arrangement among the small TiO_2 particles, consistent with previous reports of

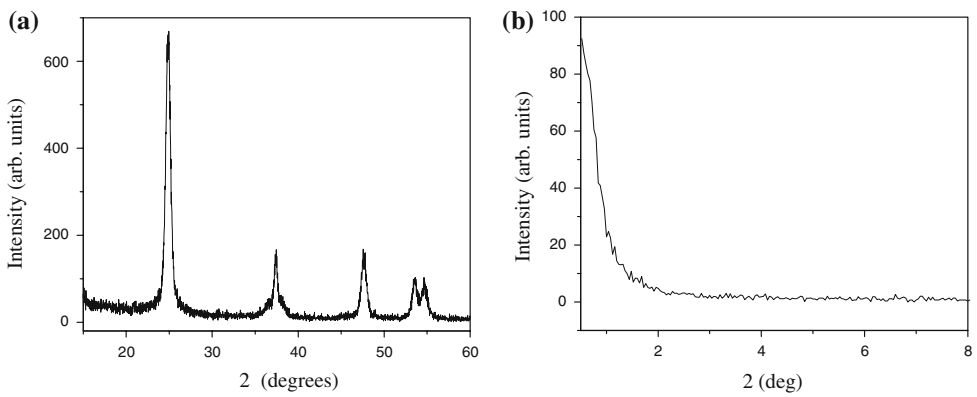

Fig. 1 Wide-angle (**a**) and low-angle (**b**) powder X-ray diffraction (*XRD*) patterns of mesoporous titania obtained after calcination at 400°C

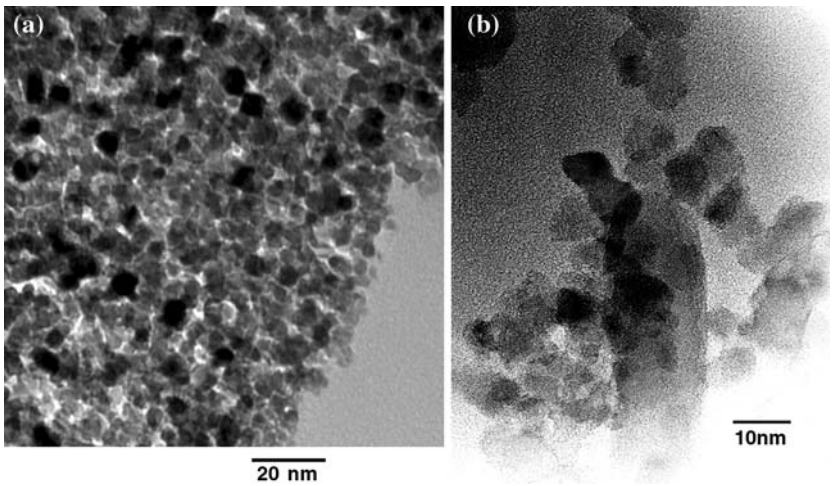

Fig. 2 (**a**) Transmission electron microscopy (*TEM*) image of mesoporous titania calcined at 400°C. (**b**) HRTEM image showing the microstructure of mesoporous titania. Lattice fringes are clearly visible for many of the particles, demonstrating their crystalline nature

worm-like pore structures [27,38]. Figure 2b shows an HR-TEM image of mesoporous titania with particles that are mostly in the size range of 5–7 nm, consistent with the XRD data. Lattice fringes are clearly visible for many of the particles, demonstrating their crystalline nature. In general, virtually no amorphous TiO_2 was found in any sample prepared during the course of the study. The worm-like pore structure formed by this synthesis may show significant photocatalytic properties due to the crystalline nature of the TiO_2 nanoparticles.

The SEM images of the TiO_2 network (Fig. 3) show that the TiO_2 is a porous network on the macroscale as well as on the mesoscale, as seen by TEM. The network is fairly homogenous with wall thicknesses of approximately 200 nm and macropore diameters that range from 100 to 500 nm. The mesopore structure, not visible on this scale, is found within the walls of the macropores. At low magnification (Fig. 3a) there is no indication of long range order. At higher magnification (Fig. 3b), however, the SEM image reveals a nearly hexagonal close packed macropore structure. The macropores allow easy access of materials to the entire mesopore network, since every part of the network is near a macropore. Thus the macropores could conceivably facilitate a catalytic process by allowing faster flow of materials through the TiO_2 network.

Figure 4 shows the N_2 adsorption–desorption isotherms of the titania sample. The isotherms of both as-prepared (Fig. 4a) and calcined (Fig. 4b) samples are of classical type IV, characteristic of mesoporous materials according to the IUPAC classification [39]. A hysteresis loop with a sloping adsorption branch and a relatively sharp steep desorption branch is observed at high relative pressure (P/P_o) range. It is well known that a distribution of various sized cavities but with the same entrance diameter would give this type of hysteresis loop. The adsorption isotherm of as-prepared sample exhibits a large increase in the P/P_o range of 0.5–0.6, which is characteristic of capillary condensation within mesopores [39].

The adsorption isotherm of TiO_2 prepared without CTAB as a template is shown in Fig. 4c. The isotherm is of classical type II, characteristic of non-porous solids. The Brunauer–Emmett–Teller (BET) surface area of this sample is 10 m^2/g and these results show that

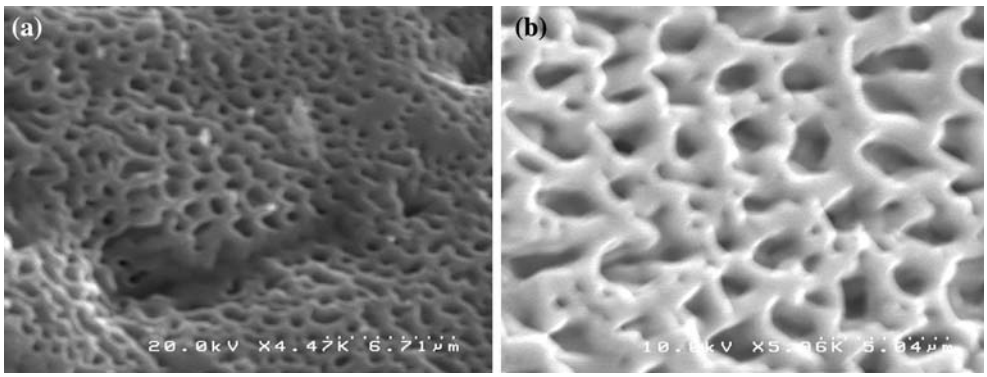

Fig. 3 Scanning electron microscopy (*SEM*) images of mesoporous titania at (**a**) low magnification and (**b**) high magnification. At higher magnification the SEM image reveals a nearly hexagonal close packed pore structure

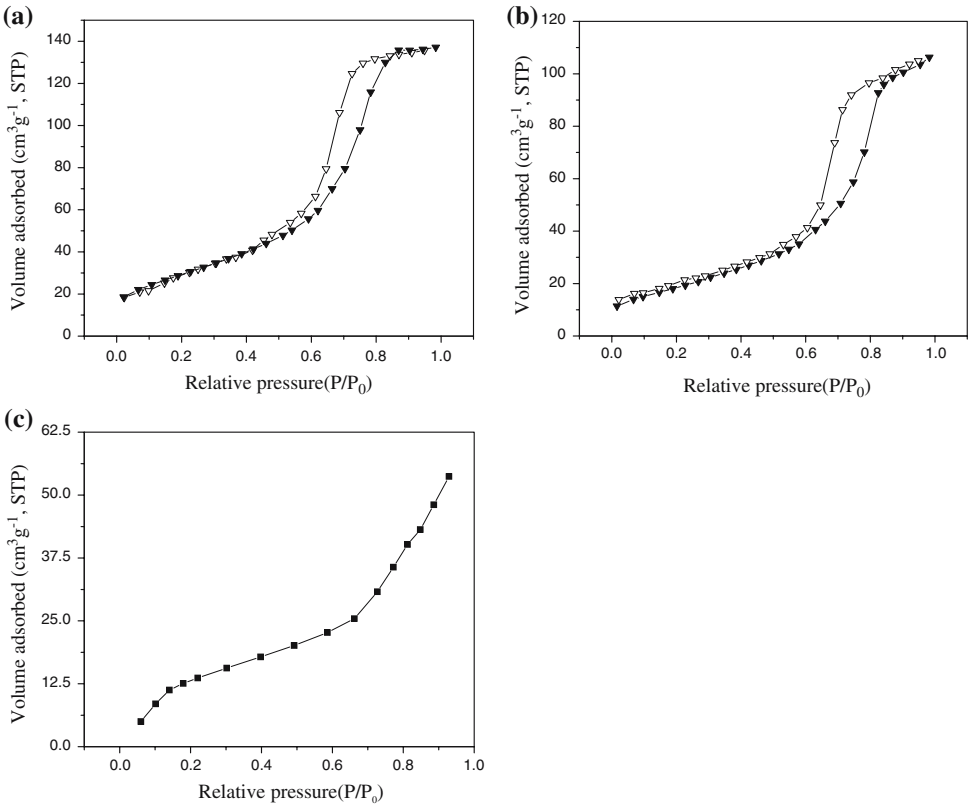

Fig. 4 Nitrogen adsorption–desorption isotherms for (**a**) as-prepared (**b**) calcined titania prepared using CTAB as a template. The adsorption isotherm of TiO_2 prepared in the absence of CTAB is shown in (**c**)

CTAB is essential for achieving a mesoporous TiO_2 network with a high surface area. The pore size distribution [determined by Barrett–Joyner–Halenda (BJH) method from the adsorption branch] of the as-prepared product is centered at 7.1 nm. After calcination at 400°C for 4 h, the position of the inflection point of as-prepared sample remained more or less at the same P/P_o range of 0.5–0.6, and the pore size reduced to 6.2 nm. The pore size distributions for both the as-prepared and calcined samples are shown in Fig. 5. The Brunauer–Emmett–Teller (BET) surface area of the product increased, however from 100 to 335 m^2/g after calcination. This is similar to the case of liquid crystal templated well-ordered mesoporous silicas having a contractible pore size after calcinations [1], thereby suggesting a mechanism of surfactant-assisted nanoparticle assembly for the formation of the mesoporous wall. The pore size distributions of both as prepared and calcined samples are quite narrow, indicating the good homogeneity of the pores.

A typical RBS spectrum for titania on a graphite substrate is shown in Fig. 6. Different species are readily identified by their position along the *x*-axis and are indicated in the plot. Notably, there is no sign of any contaminants in the titania. The only species present are O and Ti: there is no evidence of nitrogen or bromine. In the inset to Fig. 6, a scan of titania on Si(001) shows no detectable trace of carbon either, which would show up here as a peak superimposed on the Si substrate peak, similar to the observed oxygen

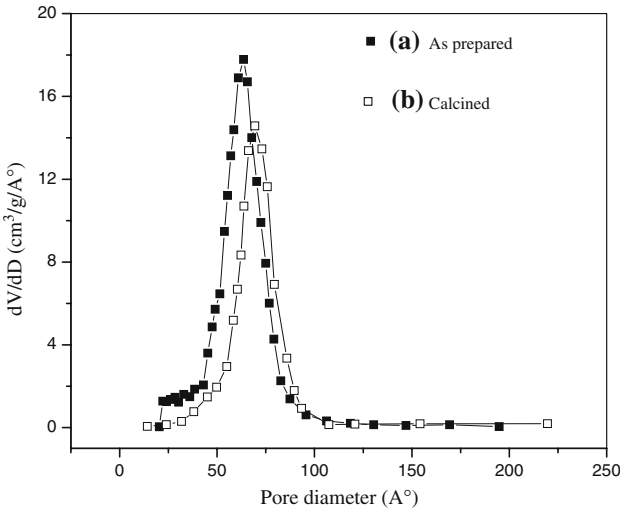

Fig. 5 Barrett–Joyner–Halenda (*BJH*) pore size distribution plots for (**a**) as-prepared and (**b**) calcined TiO_2

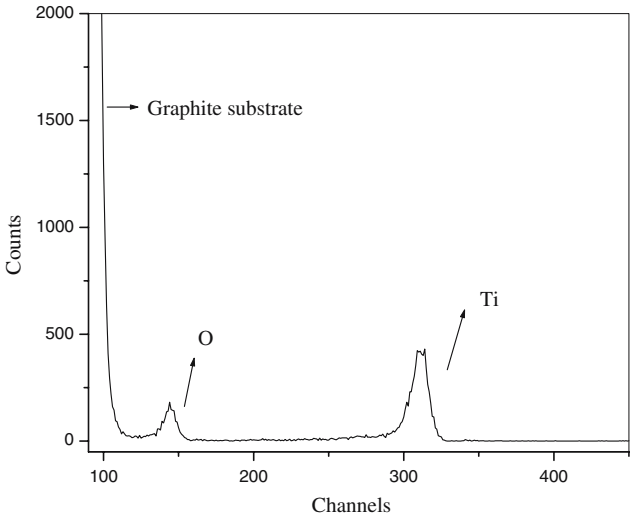

Fig. 6 Rutherford backscattering spectroscopy (*RBS*) spectrum of mesoporous titania calcined at 400°C, deposited on a graphite substrate. The *x*-axis is logarithmically related to the kinetic energy of the back-scattered helium ions.

peak. The absence of detectable contaminants shows that the calcination step has completely removed the surfactant template, leaving behind pure titania.

The RBS can also be used to determine the relative concentrations of O and Ti. The areal density (N_x) of each atomic species can be calculated by [40]

$$N_x = \frac{(A_x)(\mathrm{DTR})(C_{\mathrm{Bi}})(e)}{(Q_x)(\Omega)\left(\frac{\sigma}{\sigma_R}\right)_x(\sigma_x)} \quad (1)$$

where A_x is the area of the peak, DTR is the dead time ratio, C_{Bi} is the bismuth correction factor (determined by obtaining an RBS spectrum of a bismuth sample of known areal density), e is the elementary charge, Q_x is the total charge of the scan, Ω is the detector solid angle. The non-Rutherford correction factor, $\left(\frac{\sigma}{\sigma_R}\right)_x = 1 - \frac{0.049 Z_{\mathrm{He}} Z_x^{4/3}}{1{,}800}$ where Z_{He} is the atomic number of the incident He ions, Z_x is the atomic number of the target atom and $\sigma_x = \frac{(\sigma_R)_x}{E_{\mathrm{lab}}^2} \times 10^{-24}$ is the Rutherford cross-section. $(\sigma_R)_x$ is a tabulated value for the target atom and E_{lab} is the energy of the ion beam.

Using this formula, the ratio of Ti–O is 0.4587 ± 0.01, yielding an empirical formula for the titania of $TiO_{2.18\pm0.06}$. We attribute the excess oxygen to be coming from the surface, either through hydroxylation of the surface by the aqueous reaction conditions or through oxygenation of the surface during the calcination step of synthesis, which is conducted under O_2.

4 Conclusions

Contaminant-free, high surface area mesoporous TiO_2 with a wormhole-like framework and close-packed macropores was obtained based on a sol-gel process involving acid hydrolysis of titanium ethoxide in the presence of a cationic surfactant. The walls of the wormhole-like framework were composed of highly nanocrystalline TiO_2. At first a reaction process of alcoholysis and hydrolysis of titanium ethoxide takes place once the reactants are mixed. One possibility is that, the partially hydrolyzed titanium-oxo clusters or nanosized Ti–O particles act as primary NBB of the inorganic walls. The initial acidic media hinders immediate precipitation and grain growth of titania. The wormhole-like framework can be explained on the basis of the CTAB molecules not being able to act with sufficient cooperation to be able to impose enough curvature to the Ti-oxo growing polymers. We are exploring the possibility of using the mesoporous TiO_2 for photocatalysis and therefore the present work is currently being extended to seek alternative methods to optimize the surfactant removal while keeping the high surface areas already obtained.

Acknowledgment Funding from DOE grant No. DE FG02 02ER45957 is gratefully acknowledged.

References

1. J.S. Beck, J.C. Vartuli, W.J. Roth, M.E. Leonowicz, C.T. Kresge, K.D. Schmitt, C.T.W. Chu, D.H. Olson, E.W. Sheppard, S.B. McCullen, J.B. Higgins, J.L. Schlenker, J. Am. Chem. Soc. **114**, 10834 (1992)
2. C.T. Kresge, M.E. Leonowicz, W.J. Roth, J.C. Vartuli, J.S. Beck, Nature **359**, 710 (1992)
3. A. Stein, B.J. Melde, R.C. Schroden, Adv. Mater. **12**, 1403 (2000)
4. U. Ciesla, F. Schüth, Microporous Mesoporous Mater. **27**, 131 (1999)
5. J.Y. Ying, C.P. Mehnert, M.S. Wong Angew. Chem. Int. Ed. **38**, 56 (1999)
6. S.H. Elder, Y. Gao, X. Liu, J. Liu, D.E. McCready, C.F. Windisch Jr., Chem. Mater. **10**, 3140 (1998)
7. F. Schüth, Chem. Mater. **13**, 3184 (2001)
8. X. Hu, D. Antonelli, Angew. Chem. Int. Ed. **41**, 214 (2002)
9. Q. Huo, D.I. Margolese, U. Ciesla, P. Feng, T.E. Gier, P. Sieger, R. Leon, P.M. Petroff, F. Schüth, G.D. Stucky, Nature **368**, 317 (1994)
10. A. Monnier, F. Schüth, Q. Huo, D. Kumar, D.I. Margolese, R.S. Maxwell, G.D. Stucky, M. Krishnamurty, P.M. Petroff, A. Firouzi, M. Janicke, B.F. Chmelka, Science **261**, 1299 (1993)
11. D. M. Antonelli, J.Y. Ying, Angew. Chem. Intl. Ed. Engl., **34**, 2014 (1995)
12. A. Mills, S. Le Hunte, J. Photochem. Photobiol. A Chem. **108**, 1 (1997)

13. R. Cia, Y. Kubota, T. Shuin, H. Sakai, K. Hashimoto, A. Fujishima, Cancer. Res. **52**, 2346 (1992)
14. P. Zhang, R.J. Scrudato, G. Germano, Chemosphere **28**, 607 (1994)
15. Z. Shourong, H. Qingguo, Z. Jun, W.J. Bingkun, J. Photochem. Photobiol. A: Chem. **108**, 235 (1997)
16. S.Y. Huang, G. Schlichthörl, A.J. Nozik, M. Grätzel, A.J. Frank, J. Phys. Chem. B. **101**, 2576 (1997)
17. S.C. Luo, J.L. Falconer, J. Catal. **185**, 393 (1999)
18. L.X. Cao, Z. Gao, S.L. Suib, T.N. Obee, S.O. Hay, J.D. Freihaut, J. Catal. **196**, 253 (2000)
19. A. Hagfeldt, M. Grätzel, Chem. Rev. **95**, 49 (1995)
20. T. Moritz, J. Reiss, K. Diesner, D. Su, A. Chemseddine, J. Phys. Chem. B **101**, 8052 (1997)
21. R.L. Putnam, N. Nakagawa, K.M. McGrath, N. Yao, I.A. Aksay, S.M. Gruner, A. Navrotsky, Chem. Mater. **9**, 2690 (1997)
22. V.F. Stone Jr, R.J. Davis, Chem. Mater. **10**, 1468 (1998)
23. H. Fujii, M. Ohtaki, K. Eguchi, J. Am. Chem. Soc. **10**, 1468 (1998)
24. P. Yang, D. Zhao, D.I. Margolese, B.F. Fredrickson, B.F. Chmelka, G.D. Stucky, Science **279**, 548 (1998)
25. P. Yang, D. Zhao, D.I. Margolese, B.F. Fredrickson, B.F. Chmelka, G.D. Stucky, Nature **396**, 152 (1998)
26. D.M. Antonelli, Microporous Mesoporous Mater. **30**, 315 (1999)
27. J.Y. Zheng, J.B. Pang, K.Y. Qiu, Y. Wei, J. Mater. Chem. **11**, 3367 (2001)
28. Y. Wang, X. Yang, L. Yin, W. Huang, Y.R. Hacohen, A. Gedanken, Adv. Mater. **12**, 1183 (2000)
29. D. Grosso, G.J.D.A.A. Soler-Illia, F. Babonneau, C. Sanchez, P.-A. Albouy, A.B. Bruneau, A.R. Balkenende, Adv. Mater. **13**, 1085 (2001)
30. G.J.D.A.A. Soler-Illia, A. Louis, C. Sanchez, Chem. Mater. **14**, 750 (2002)
31. E.L. Crepaldi, G.J.D.AA. Soler-Illia, D. Grosso, F. Cagnol, F. Ribot, C. Sanchez, J. Am. Chem. Soc. **125**, 9770 (2003)
32. G.J.D.A.A. Soler-Illia, C. Sanchez, B. Lebeau, J. Patarin, Chem. Rev. **102**, 4093 (2002)
33. K. Cassiers, T. Linssen, V. Meynen, P. Van Der Voort, P. Cool, E.F. Vansant, Chem. Commun. 1178 (2003)
34. K. Cassiers, T. Linssen, M. Mathieu, Y.Q. Bai, H.Y. Zhu, P. Cool, E.F. Vansant, J. Phys. Chem. B **108**, 3713 (2004)
35. E. Beyers, P. Cool, E.F. Vansant, J. Phys. Chem. B, **109**, 10081 (2005)
36. K. Cassiers, T. Linssen, K. Aerts, P. Cool, O. Lebedev, G. Van Tendeloo, R. Van Grieken, E.F. Vansant, J. Mater. Chem. **13**, 3033 (2003)
37. A. Firouzi F. Atef A.G. Oertli G.D. Stucky B.F. Chmelka, J. Am. Chem. Soc. **119**, 3596 (1997)
38. T.Z. Ren, Z.Y. Yuan, B.L. Su, Chem. Phys. Lett. **374**, 170 (2003)
39. K.S.W. Sing, D.H. Everett, R.A.W. Haul, L. Moscow, R.A. Pierotti, J. Rouquerol, T. Siemieniewska, Pure Appl. Chem. **57**, 603 (1985)
40. J.R. Tesmer M. Natasi, *Handbook of Modern Ion Beam Materials Analysis*, (Materials Research Society, Pittsburgh, PA, 1995)